Microstructure and Micro-Hardness Properties of In-Situ LENS Fabricated Ti-Al-Si-xV Alloys

Sadiq Abiola Raji[1,2,*], *Abimbola Patricia Idowu* Popoola[1], *Sisa* Pityana[3], *Olawale Muhammed* Popoola[4] and *Monnamme* Tlotleng[3,5]

[1]Department of Chemical, Metallurgical and Materials Engineering, Tshwane University of Technology, Staatsartillerie Road, Pretoria West, Pretoria, South Africa
[2]Department of Metallurgical Engineering, Yaba College of Technology, P.M.B. 2011 Yaba, Lagos, Nigeria
[3]National Laser Centre, Council for Scientific and Industrial Research (NLC-CSIR), Meiring Naude Road, Pretoria, South Africa
[4]Department of Electrical Engineering, Centre for Energy and Electric Power (CEEP), Tshwane University of Technology, Staatsartillerie Road, Pretoria West, Pretoria, South Africa
[5]Department of Mechanical Engineering Science, University of Johannesburg, Auckland Park Campus, Johannesburg, South Africa

Abstract. This study presents laser in-situ alloying of Ti-Al-Si-xV alloys fabricated using the laser engineered net shaping (LENS) machine from elemental powders. The as-built samples were subjected to heat treatment at 1200°C, 1300°C, and 1400°C for 1 hour and furnace cooled (FC) with subsequent homogenization heat treatment at 950°C for 6 hours and FC. The microstructure was characterized by scanning electron microscopy (SEM) equipped with an electron dispersion spectroscopy (EDS). The micro-hardness properties were evaluated with the Vickers hardness tester. The results showed that alloying via in-situ powder deposition followed by heat treatment is practicable for the producing TiAl-based alloys with improved mechanical properties.

1 Introduction

The main advantage of additive manufacturing (AM) over conventional manufacturing routes is high precision of manufactured parts [1]. This class of technology includes directed energy deposition (DED) AM, also known as laser engineered net shaping (LENS). In the past couple of years, materials such as metals, composites, ceramics, and functionally graded materials (FGM) including titanium aluminide-based alloys (TiAl-based) have been successfully processed using LENS technique [1-5]. Despite the fact that several alloys have been used to fabricate superior engineering structures, the fabrication of superior structures with TiAl intermetallic alloys has proven to be problematic.

Owing to combined unique physical, chemical, and mechanical properties that make titanium alloys uniquely suitable for the aerospace, marine, and chemical industrial sectors. Titanium alloys have widely been used for a variety of applications with respect to aerospace,

* Corresponding author: RajiSA@tut.ac.za; rajisadiqa@gmail.com

marine, and chemical industries [3,6]. As a result, TiAl-based alloys have been developed for use in structural and aerospace applications due to their attractive properties such as low density, high modulus and high temperature strength [3]. However, improved ductility and fracture toughness through microstructure and alloy control have received much attention to improve the properties of TiAl-based alloys.

Due to its excellent strength-to-weight ratio, high specific modulus, and good creep resistance, the intermetallic alloy γ-TiAl has a growing interest for elevated temperature applications in the aerospace, automotive, and power generation industries [7-9]. Significant progress has been made in the past decade to improve its room-temperature (RT) ductility and high-temperature (>850◦C) oxidation resistance by alloy modifications, processing, innovations and surface engineering [10-11]. Several authors have also suggested micro-alloying addition such as Mo, Nb, Cr and Si to improve mechanical properties of TiAl alloys [3-4,12-16]. Nevertheless, inadequate hot workability is still a foremost issue regarding TiAl alloys which has led to a lot of interests from researchers in trying to mitigate the associated drawbacks confronting the wider application of this type of material [4].

According to Raji et al. [3], alloying elements aimed at improving mechanical properties include V, Nb, Ta, Mo, Cr, Mn and W for enhanced ductility and stabilizing β-phase in the microstructure of γ-TiAl-based alloys. They also help to increase their fracture toughness at RT; while B, C and Si are for microstructural refinement [3]. It has been observed by Ye et al. [17], that V tends to show stronger β-stabilizing effects than Nb and Ta. Although V, Nb and Ta contain similar valence of electrons [17]. Thus, the β-stabilizing effects is not a function of the number of valence electrons. It was also reported that alloying elements with a smaller atomic radius such as Mn, V, and Cr leads to more stable β-phase formation [3,17]. Cui et al. [18], reported that alloys produced by Cr, Mn, and V have β-phase with low hardness; while Nb, Mo, or W results in β-phase of higher hardness values. Hence, the reduction of hardness through alloying could be employed in designing compositions of β-solidifying TiAl-based alloys with excellent RT ductility.

TiAl alloys containing Si are potential materials for elevated temperature utilization in the aerospace and automobile industries. However, the addition of Si in TiAl-based alloys as an alloying element is often controversial. Most discussions available in literature are usually on microstructural stability and creep resistant associated with Si addition [19-20]. Nevertheless, Si is known to be a highly promising alloying element for improving elevated temperature strength of Ti–Al alloy systems [21-22]. This is due to the Ti_5Si_3-phase (ζ-silicide; HCP structure) formed that acts as a strengthening phase for composites' reinforcement based on TiAl intermetallic alloys [3,5].

Some advanced TiAl alloys are now nearly maturing to the stage where it is possible to implement them for industrial applications. As a new generation of light weight, elevated-temperature candidate of structural materials, the mechanical properties need to be enhanced, especially when applied as components such as shafts, blades in gas turbines and exhaust valves in internal combustion engines, in which performance in service are critically important to the component's performance. In our previous study [5], the microstructure and mechanical properties of ternary Ti-Al-Si alloy produced through in-situ laser processing using the LENS machine was investigated. On the other hand, there are limited or no literature and information on the effects of V additions on ternary Ti-Al-Si alloys.

In this present study, we focus on preparing the compositionally graded TiAl-based (Ti-Al-Si-xV) intermetallic alloys through the LENS in-situ powder deposition and adjustment of the feeding rate of V during laser powder deposition. Three graded TiAl-based intermetallic alloys were obtained. Microstructure characterization and composition distribution of the graded TiAl-based intermetallic alloys were analysed by scanning electron microscopy (SEM) equipped with electron dispersion spectroscopy (EDS). The hardness

distributions of the graded TiAl-based intermetallic alloys were also investigated by the Vickers hardness tester.

2 Methodology

The Optomec 850R LENS machine with 1 kW IPG fibre laser was used to fabricate the samples of Ti-Al-Si-xV alloys with different atomic weight percent (at.%) of V. This machine uses an IPG fiber laser as energy source and argon gas to maintain the inert environment. It uses a deposition head with four copper feeding nozzles and a workstation with the computer software program. Two of the powders (Ti and Al) were delivered from the hoppers of the Optomec machine while the other powders (Si and V) were fed from a GTV powder hopper externally attached onto the other hoppers of the LENS machine. The SEM secondary electron images (SEIs) of the metal powders used are presented in Fig. 1.

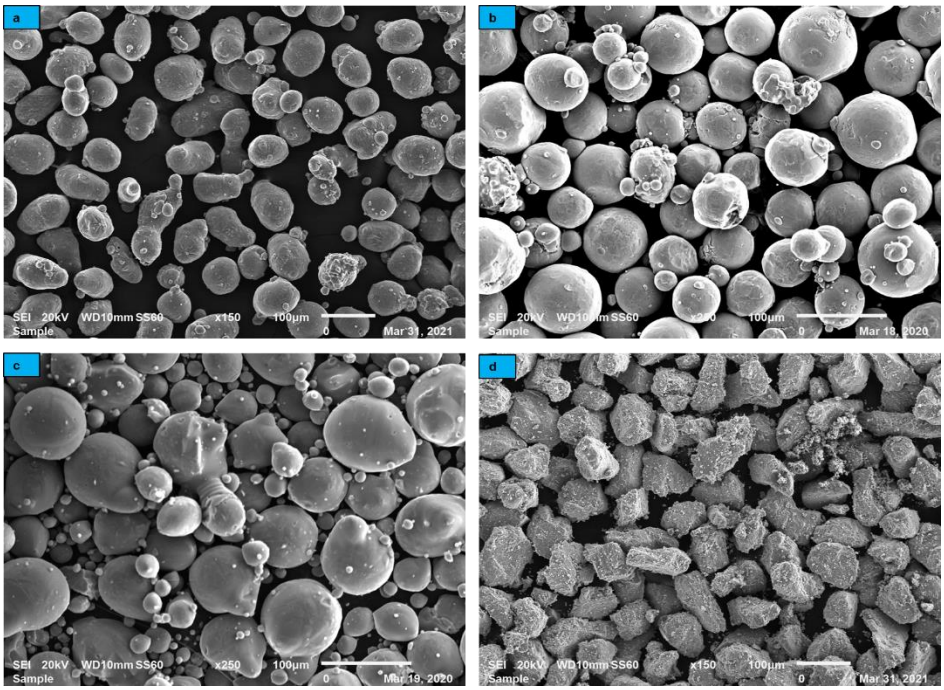

Fig. 1. SEIs of (a) Al, (b) Ti, (c) Si and (d) V powder sample

The specimens were fabricated based on a pre-programmed CAD file loaded with the workstation software of the Optomec application version 3.1.6 which automatically controls and operate the deposition head. Spherical shaped powders from TLS Technik GmbH & Co of 45-90 µm particle size were used in this study. The samples were built on Ti-6Al-4V alloy substrate plate without any pre-heating. Sample cubes of 15 mm by 15 mm by 10 mm was built with build parameters listed in Table 1. The process set-up adopted in this study is similar as in ref [5,23] with the optimized processing parameters as indicated in Table 1. The as-produced specimen cubes were heat treated at a rate of 500 ^{o}C/hour in an argon-rich environment at three different temperatures of 1200 ^{o}C, 1300 ^{o}C, and 1400 ^{o}C for 1 hour and furnace cooled (FC) at 100 ^{o}C/hour. This was followed by homogenization heat treatment at 950 ^{o}C for 6 hours and FC.

Table 1: Parameters used for in-situ LENS deposition for the quaternary Ti-Al-Si-xV alloys

Parameter	***Values***			
Laser Power (W)	450 W			
Scan Speed (mm/s)	10.58 mm/s			
Hatching spacing (mm)	2.5 mm			
Layer thickness (mm)	5 mm			
Centre Purge (l/min)	25 l/min			
	Ti	Al	Si	V
Carrier gas (l/min)	4.2	2.4	2.0	2.0
Powder Feed Rate (g/min)	2.21	0.48	0.03	0.18
				0.33
				0.49

The cube samples of the LENS fabricated Ti-Al-Si-xV alloys were sectioned transversely along the builds. Prior to performing morphological characterization, surfaces of the samples were mechanically ground and polished using standard metallographic procedures. After etching with Kroll's reagent (2% HF, 6% HNO_3 92% distilled water all in volume fractions) allows the microstructures to be visibly examined by using SEM equipped with EDS. Micro-hardness measurement was carried out using Zwick/Roell Indentec (ZHVμ) Vickers micro-hardness tester. Diamond indenter with pyramidal shape having an angle of 136^o between opposite faces was used. A load of 500 gf with dwell time of 10 s was applied for the indentation. The micro-hardness was measured at 15 different locations and the average value was calculated.

3 Results and Discussions

3.1 Microstructure of graded Ti-Al-Si-xV Alloys

The SEIs in Fig. 2 presents the as-built Ti-Al-Si-xV alloys processed with 0.18 g/min, 0.33 and 0.49 g/min V additions and the compositions are shown in Table 2. It has been reported by Appel, Paul and Oehring [24], that V moves the (α_2+γ)/γ lamellae towards the Ti dominated area thereby improving the ductility of TiAl-based alloys and reducing the Al content in the γ phase. These quaternary alloys of Ti-Al-Si-xV demonstrate (α_2+γ)/γ dominating the microstructure prompted by the V additions in the alloy. The SEM image in Fig. 2 corresponds to 5.11 at.%, 9.42 at.% and 10.78 at.% for the Ti-Al-Si-xV alloys with 0.18 g/min, 0.33 and 0. 49 g/min V additions, respectively. This is because of the low Al content that predominantly favours α_2-Ti_3Al phase in the microstructures of TiAl-based alloys. Although the alloys had (α_2+γ)/γ lamellae, ζ-Ti_5Si_3 that are visible around the grain boundaries, it is still embedded within the α_2-phases.

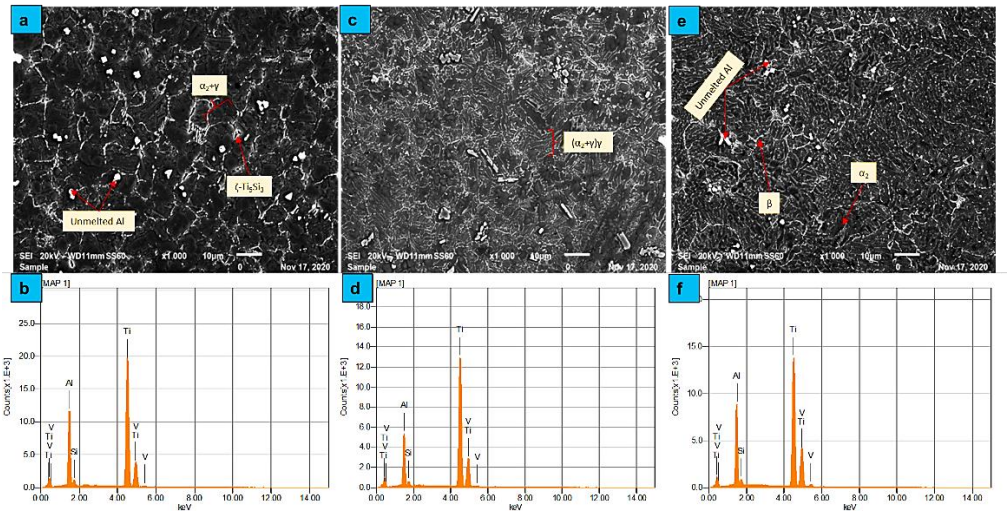

Fig. 2. The SEIs and EDS images of as-built Ti-Al-Si-xV alloys processed at (a), (b) 0.18 g/min, (c), (d) 0.33 g/min, (e), (f) 0.49 g/min, respectively

Table 2. Composition of as-built Ti-Al-Si-xV Alloys

	Al (at.%)	***Si (at.%)***	***Ti (at.%)***	***V (at.%)***
0.18 g/min V	39.32±1.00	1.98±0.04	53.59±1.80	5.11±0.11
0.33 g/min V	36.71±2.60	2.10±0.38	51.77±1.27	9.42±0.62
0.49 g/min V	36.59±2.51	1.95±0.02	50.68±1.14	10.78±0.04

The heat treatment carried out on the Ti-Al-Si-xV alloys was done on all the as-built alloys. The SEIs and EDS images is shown in Fig. 3, Fig. 4 and Fig. 5; while the compositions of the Ti-Al-Si-xV alloys are presented in Table 3. The phases identified in the heat-treated Ti-Al-Si-xV alloy samples are $\alpha_2+\gamma/\gamma$, β and ζ-Ti_5Si_3 phases. These phases are similar to the as-built alloys, however, the $\alpha_2+\gamma/\gamma$ lamellae was more obvious with smaller quantities of β-phase formed after heat treatment. It was perceived that the strategy adopted for heat treating these alloys resulted in the over refinement of the microstructure. Thereby, further decreasing the amount of $\alpha_2+\gamma/\gamma$ at higher temperatures owing to a reduction in Al content. This was easily detected for all samples heat-treated at 1400ºC/60 mins/FC/950ºC/6 h/FC as compared to those ones at 1200ºC/60 mins/FC/950ºC/6 h/FC that formed more $\alpha_2+\gamma$ colonies. Since V is not a strong β-stabilizer like Mo, the ζ-Ti_5Si_3 was able to dissolve most of the β formed in the α_2-matrix.

Generally, the heat-treated samples have lesser Al content when compared to their as-built alloys noticed in Table 3. The composition of Si and V stays almost the same like their as-built alloys notwithstanding the heat treatment conditions but the Al content reduces in all the heat-treated alloy samples. This promotes α_2 phase formation that serves as nucleation sites for both β and ζ phases. Therefore, dissolution of the β phase was accomplished owing to the presence of ζ-phase and V being a weak β-stabilizer. Besides, all the heat-treated samples only showed a slight variation in Si content. Hence, promoting the ζ-Ti_5Si_3 phase formation in the α_2 phase which results in the decrease of β phase formed.

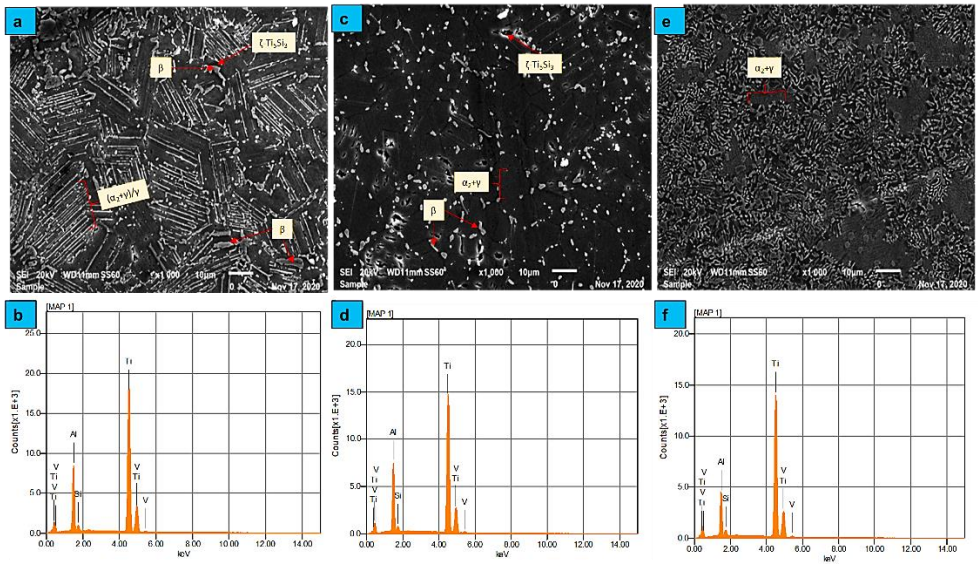

Fig. 3. SEIs and EDS images of Ti-Al-Si-0.18 g/min V heat treated at (a), (b) 1200ºC/60 mins/FC/950ºC/6 h/FC, (c), (d) 1300ºC/60 mins/FC/950ºC/6 h/FC and (e), (f) 1400ºC/60 mins/FC/950ºC/6 h/FC, respectively

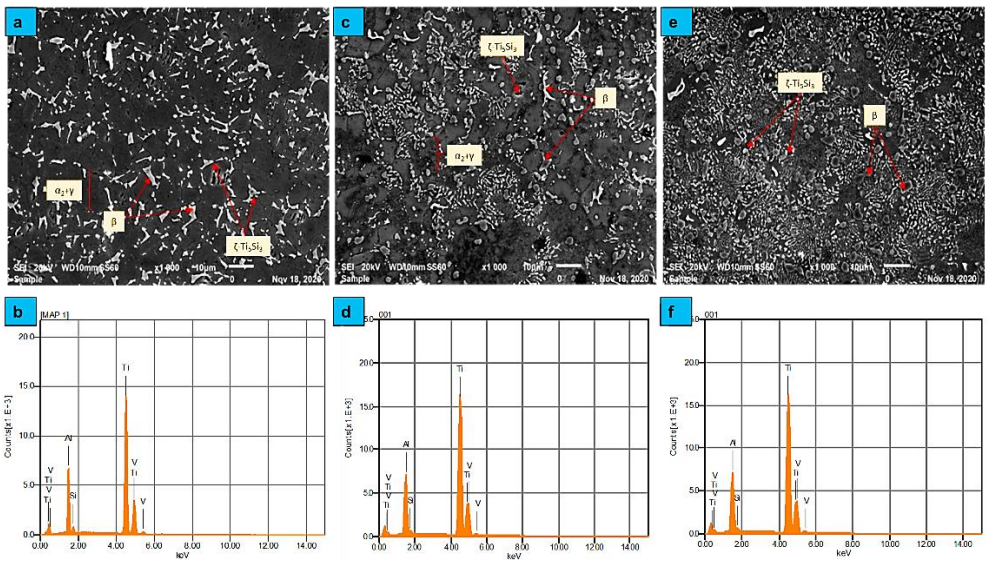

Fig. 4. SEIs and EDS images of Ti-Al-Si-0.33 g/min V heat treated at (a), (b) 1200 ºC/60 mins/FC/950 ºC/6 h/FC, (c), (d) 1300 ºC/60 mins/FC/950 ºC/6 h/FC and (e), (f) 1400 ºC/60 mins/FC/950 ºC/6 h/FC, respectively

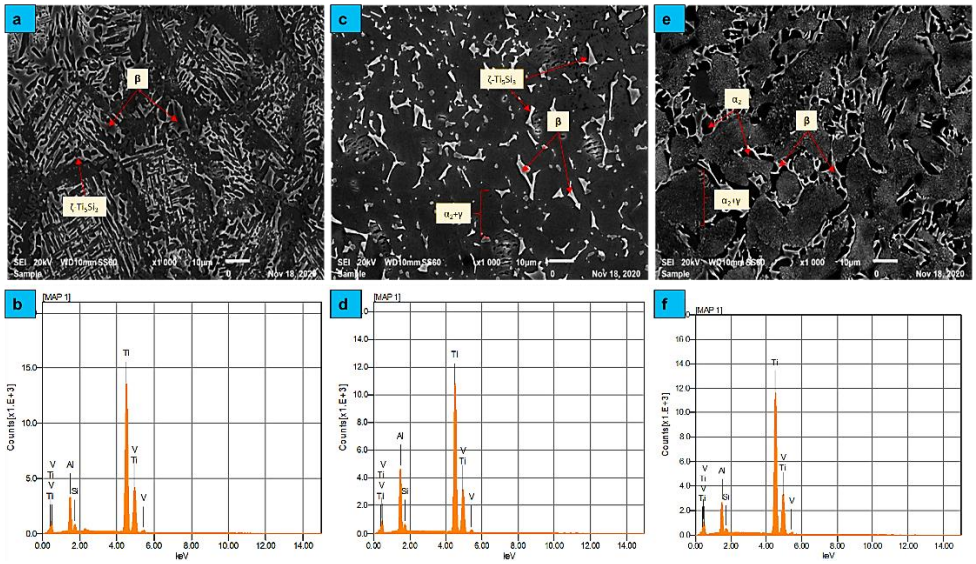

Fig. 5. SEIs and EDS images of Ti-Al-Si-0.49 g/min V heat treated at (a), (b) 1200ºC/60 mins/FC/950ºC/6 h/FC, (c), (d) 1300ºC/60 mins/FC/950ºC/6 h/FC and (e), (f) 1400ºC/60 mins/FC/950ºC/6 h/FC, respectively

Table 3: Composition of heat-treated Ti-Al-Si-xV alloys

	Heat Treatment Conditions	***Al (at.%)***	***Si (at.%)***	***Ti (at.%)***	***V (at.%)***
0.18 g/min of V	1200ºC/60 mins/FC/950ºC/6 h/FC	37.71±0.90	2.16±0.10	54.70±0.80	5.43±0.22
	1300ºC/60 mins/FC/950ºC/6 h/FC	37.86±0.14	1.92±0.04	55.09±0.31	5.13±0.20
	1400ºC/60 mins/FC/950ºC/6 h/FC	36.50±0.88	2.39±0.02	55.35±0.95	5.76±0.30
0.33 g/min of V	1200ºC/60 mins/FC/950ºC/6 h/FC	35.87±0.20	2.05±0.01	53.59±0.10	8.49±0.30
	1300ºC/60 mins/FC/950ºC/6 h/FC	33.03±1.89	2.31±0.57	55.66±1.95	9.00±0.88
	1400ºC/60 mins/FC/950ºC/6 h/FC	31.32±0.52	1.94±0.00	57.71±1.60	9.03±0.22
0.49 g/min of V	1200ºC/60 mins/FC/950ºC/6 h/FC	31.02±1.30	2.36±1.12	52.61±1.14	14.01±0.04
	1300ºC/60 mins/FC/950ºC/6 h/FC	33.61±1.14	2.21±0.14	52.82±0.55	11.36±0.38
	1400ºC/60 mins/FC/950ºC/6 h/FC	31.24±0.29	1.67±0.08	53.14±1.05	13.95±1.25

The microstructure of the as-built Ti-Al-Si-xV alloy with 0.33 g/min of V shows a clearer representation of the morphological features of the fabricated alloy. The darker region depicts an Al-rich area, whereas the composition of the bright sections represents areas of lower Al content. The white precipitates detected in the alloys is composed primarily of α_2-Ti_3Al and ζ-Ti_5Si_3. The equiaxed α_2/γ lamellae colonies particles comprise largely $\alpha_2+\gamma/\alpha_2$ structures due to limited amount of Al content. Consequently, the higher feed rate of V leads to increased quantities of β and ζ-Ti_5Si_3 contents of both as-built and heat-treated samples.

For the heat-treated samples with more than 2 at.% of Si, the hexagonal phase ζ-Ti_5Si_3 primarily solidifies from the matrix which consists of the eutectic $\alpha_2+\zeta$-Ti_5Si_3. The quantity of primary precipitated ζ-Ti_5Si_3 in the matrix increases with increasing Si content. This is caused by the present of the β phase that is precipitated from the grain boundary interface that acts as nucleation sites during the solidification of TiAl phases leading to an equiaxed microstructure. Annealing at a temperature of 950ºC results in homogenization of the alloys

and an increase in microstructural stability. However, the heat treatment strategy adopted does not reduce the amount of precipitate phases formed in comparison to the as-built alloys.

Generally, laser AM processing gives rise to rapid solidification which can cause the segregation of various elements. However, the fast solidification rate avoids the coarsening of the TiAl-based unlike traditional methods [1,5-6]. Equiaxed α_2 is present in some areas and absent in those areas where growth of γ phase occurs. This implies that presence of α_2 dominate the solidification stage, hindering the formation of γ. This is visible in SEIs (Fig. 3, Fig. 4 and Fig. 5). According to Ti-Al phase diagram, the solidification takes place in the eutectic zone. During the solidification the expected phases to be in equilibrium are α_2+γ matrix with inhomogeneous distribution of β+ζ precipitates. AMed samples experiences at least 3 solid-liquid cycles along with heat treatments consecutively at temperatures above β transformation coarsening the phase.

However, these observations are valid where β+ζ concentration was almost absent. This confirms that V distribution rather than the amount, volume or size is important during grain refinement of β+ζ. The α_2-phase are known to have limited coarsening even at high temperatures [5]. This also prevents the coarsening of lamellar grains. In summary, the microstructure of the heat-treated Ti-Al-Si-xV alloys showed different morphological features from the as-built samples with refined equiaxed grains as the V content increases in the deposits. The formation of hard β and ζ-Ti_5Si_3 was more predominant at the grain boundaries.

3.2 Micro-hardness of graded Ti-Al-Si-xV Alloys

Fig. 6 shows the distribution of the microhardness for the as-built Ti-Al-Si-xV alloys. It was inferred that V additions leads to reduction the micro-hardness values of the Ti-Al-Si-xV alloys. The highest average microhardness value is approximately 675 $HV_{0.5}$ corresponding to a YS of 2207 MPa (using Equation 1 in ref [5]). This is much lower than the values achieved in our previous works for Ti-Al-0.43 g/min Si [5] and Ti-Al-0.03 g/min Si-xMo [4] alloys. Thus, it depicts that V additions would improve the fracture toughness and ductility of typical TiAl-based alloys. All the same, the micro-hardness values obtained for further V additions above 0.49 g/min (not presented in this work) resulted in considerably high micro-hardness values with desirable microstructures and composition for consideration as TiAl-based alloys. Therefore, adding V can demonstrate both positive and negative behaviours on mechanical properties of TiAl-based alloys. This may necessitate including other alloying elements of small quantities to stabilize the microstructure and balance this drawback.

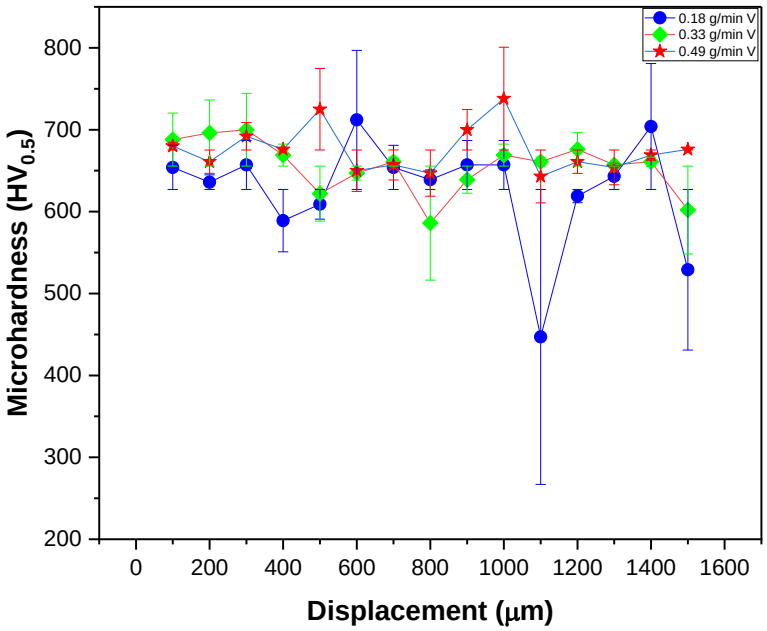

Fig. 6. Micro-hardness of as-built Ti-Al-Si-xV alloys

Fig. 7, Fig. 8 and Fig. 9 presents the distribution of the microhardness of the heat-treated Ti-Al-Si-xV alloys fabricated at 0.18 g/min, 0.33 g/min and 0.49 g/min V additions, respectively and the average microhardness values are presented in Table 4. Generally, the microhardness values of all the heat-treated alloys increases with temperature and the 1400ºC heat-treated samples showing the highest microhardness values regardless of the amount of V deposited; while the hardness values of the 1200ºC and 1300ºC for 0.18 g/min and 0.49 g/min V additions were relatively close. This was credited to the Al content (<40 at.%) which supports formation of more α_2 enabling high precipitation of ζ-Ti_5Si_3 phases. It is understood that the ζ-Ti_5Si_3 phase is the hardest phase present in the microstructure of the Ti-Al-Si-xV alloys resulting on increased micro-hardness values.

Generally, the average microhardness values of the heat-treated Ti-Al-Si-xV alloys were all above 630 $HV_{0.5}$ irrespective of V additions which tallies to a YS of approximately 2060 MPa. This establishes that even though V addition decreases the microhardness, these values were still quite high owing to the lower Al content and presence of Si that promoted ζ-Ti_5Si_3 phase formation in the presence of α_2. Thus, it is necessary to decrease Si while retaining the amount of V added as alloying element to diminish the detrimental effects on the mechanical properties.

The high hardness of the heat-treated Ti-Al-Si-xV alloys is attributable to the formation of β and ζ-Ti_5Si_3 phase and excess amount of alloying elements in the solid solution phase. Conversely, the hardness of the as-built alloys were lesser due to relatively high amount of Al in the alloy compositions. According to the Archard's law, increased hardness generally improves the wear resistant properties of a material [25-26]. The microhardness values were observed to increase with increase in V feed rate. This was expected because of the increase in β and ζ-Ti_5Si_3 phase precipitating randomly and dispersedly distributed causing the strengthening of the alloys. From the work of Mathabathe, Modiba and Bolokang [14], it is understood that based on Hall-Petch relationship that hardness values are inversely proportional to the microstructure grain size. Thus, in this work the variation in micro-hardness can be attributed to the influence and distribution of the strengthening phases on the microstructures. The addition of V could increase the wear resistance and reduce the friction

coefficient because of the dispersion hardening of the β phase. In general, materials with a high hardness possess excellent wear resistance.

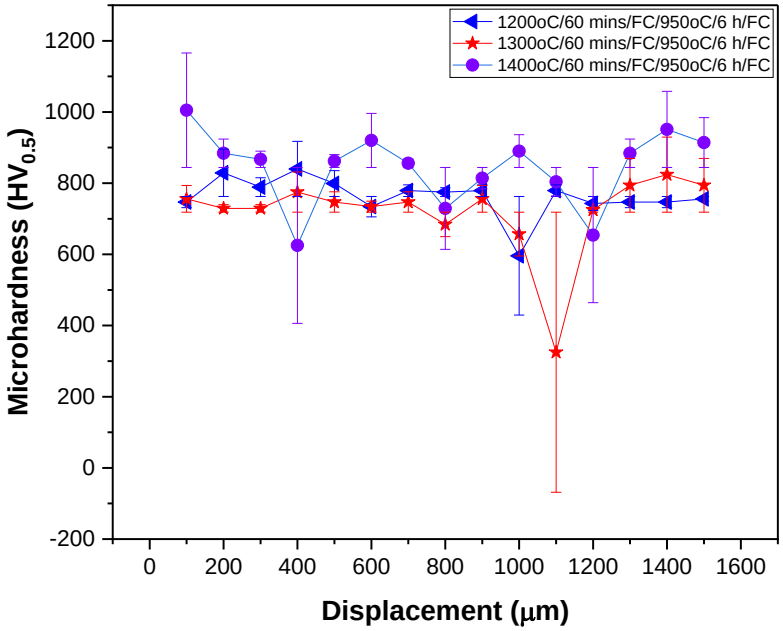

Fig. 7. Micro-hardness of heat-treated Ti-Al-Si-0.18 g/min V alloys

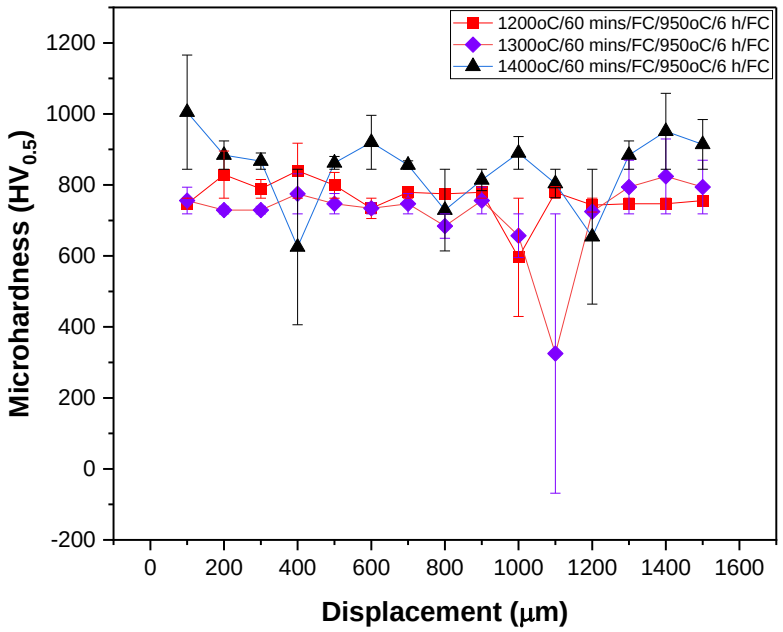

Fig. 8. Micro-hardness of heat-treated Ti-Al-Si-0.33 g/min V alloys

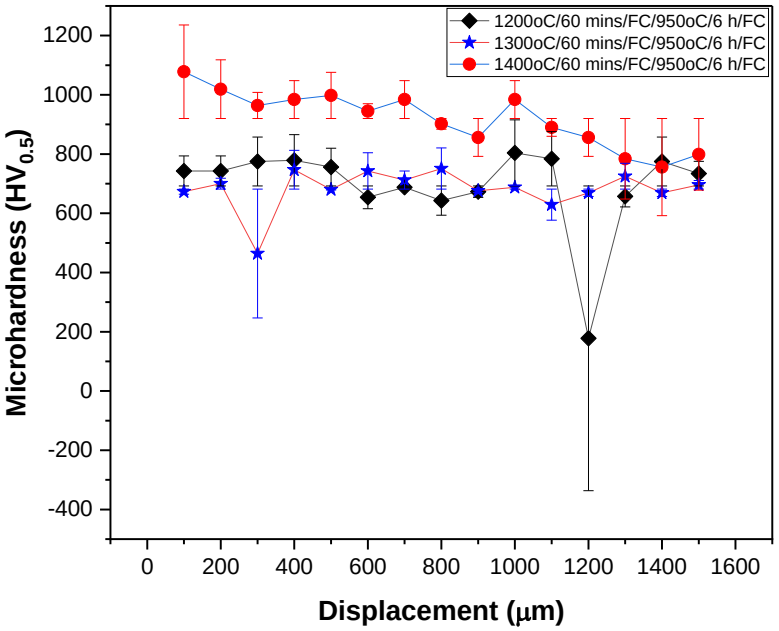

Fig. 9. Micro-hardness of heat-treated Ti-Al-Si-0.49 g/min V alloys

It is generally known that ζ-Ti_5Si_3 has some outstanding advantages. These include a high melting point, a low density, high hardness, excellent wear resistance, high thermal stability and excellent high temperature oxidation resistance [3,10,14,22]. This means that ζ-Ti_5Si_3 is an excellent reinforced phase for wear-resistance and oxidation-resistance. It can also be seen that the hardness of these alloys increases with an increase of V content. With the highest values in samples heat-treated at 1400ºC/60 mins/FC/950ºC/6 h/FC due to the slow cooling (100 ºC/hour) rate that allows for complete transformation of β and ζ-Ti_5Si_3 phases. However, micro-hardness values of the as-built alloys were lesser because of the rapid heating and cooling effects in the LENS process, thereby, leaving little time for full transformation of the precipitating phases of β and ζ-Ti_5Si_3.

Table 4: Average microhardness values for the LENS fabricated Ti-Al-Si-xV alloys

	Heat Treatment Conditions	***Microhardness ($HV_{0.5}$)***
0.18 g/min V	As-Built	627.0667
	1200ºC/60 mins/FC/950ºC/6 h/FC	762.6
	1300ºC/60 mins/FC/950ºC/6 h/FC	718.4
	1400ºC/60 mins/FC/950ºC/6 h/FC	843.9333
0.33 g/min V	As-Built	655.6
	1200ºC/60 mins/FC/950ºC/6 h/FC	635.4
	1300ºC/60 mins/FC/950ºC/6 h/FC	805
	1400ºC/60 mins/FC/950ºC/6 h/FC	856.5333
0.49 g/min V	As-Built	675.2667
	1200ºC/60 mins/FC/950ºC/6 h/FC	692.4
	1300ºC/60 mins/FC/950ºC/6 h/FC	681.4667
	1400ºC/60 mins/FC/950ºC/6 h/FC	919.9333

4 Conclusions

The study carried out via laser in-situ alloying to develop a Ti-Al-Si-xV alloys with LENS techniques was attained. A dual-stage heat treatment was performed on the fabricated alloy samples and ensuing microstructures were studied. The most significant results can be summarized as follows:

1. The fabrication of Ti-Al-Si-xV alloys by means of LENS techniques reveals that the development of TiAl-based alloys from their elemental powders called in-situ alloying was possible and attainable.
2. The alloys basically contain the phases of α_2-Ti_3Al, γ-TiAl, β-TiAl and ζ-Ti_5Si_3 in the microstructure obtained.
3. The two-step heat treatments lead to reduction in Al content, thereby decreasing α_2/γ colonies and promoting ζ-Ti_5Si_3 formation in the presence of α_2.
4. The micro-hardness values of the heat-treated Ti-Al-Si-x V alloys were above 630 $HV_{0.5}$ regardless of the V content. It was established that the microhardness values were significantly affected by the lower Al content and presence of Si that promoted ζ-Ti_5Si_3 phase.

References

1. D. Svetlizky, B. Zheng, T. Buta, Y. Zhou, O. Golan, U. Breiman, R. Haj-Ali, J.M. Schoenung, E.J. Lavernia, N. Eliaz, M&D **192**, 108763 (2020) https://doi.org/10.1016/j.matdes.2020.108763
2. S.A. Raji, A.P.I. Popoola, S.L. Pityana, O.M. Popoola, F.O. Aramide, M. Tlotleng, N.K.K. Arthur, In: Mofid Gorji-Bandpy, M and Aly, A (Eds), Aerodynamics 2019, IntechOpen, London, 193-218 (2019) https://doi.org/10.5772/intechopen.85538
3. S.A. Raji, A.P.I. Popoola, S.L. Pityana, O.M. Popoola, Heliyon **6**, e04463 (2020) https://doi.org/10.1016/j.heliyon.2020.e04463
4. S,A. Raji, A.P.I. Popoola, S.L. Pityana, O.M. Popoola, N.K.K. Arthur, M. Tlotleng, SATN **40**, 91-97 (2021) https://hdl.handle.net/10520/ejc-aknat_v40_n1_a34
5. S.A. Raji, A.P.I. Popoola, S.L. Pityana, M. Tlotleng, JMEP **30**, 3321–3332 (2021) https://doi.org/10.1007/s11665-021-05681-9
6. L.E. Murr, S.M. Gaytan, A. Ceylan, E. Martinez, J.L. Martinez, D.H. Hernandez, B.I. Machado, D.A. Ramirez, F. Medina, S. Collins, R.B. Wicker, Acta Mat. **58**, 1887-1894 (2010) https://doi.org/10.1016/j.actamat.2009.11.032
7. P. Erdely, P. Staron, E. Maawad, N. Schell, H. Clemens, S. Mayer, Acta Mat. **158**, 193-205 (2018). https://doi.org/10.1016/j.actamat.2018.07.062
8. M. Seifi, A.A. Salem, D.P. Satko, U. Ackelid, S.L. Semiatin, J.J. Lewandowski, Jallcom **729**, 1118-1135 (2017) https://doi.org/10.1016/j.jallcom.2017.09.163
9. A. Seidel, S. Saha, T. Maiwald, J. Moritz, S. Polenz, A. Marquardt, J. Kaspar, T. Finaske, E. Lopez, F. Brueckner, C. Leyens, Jom **71**, 1513-1519 (2019) https://doi.org/10.1007/s11837-019-03382-2
10. M. Kastenhuber, T. Klein, H. Clemens, S. Mayer, Intermet **97**, 27-33 (2018) https://doi.org/10.1016/j.intermet.2018.03.011

11. H.R. Jiang, Z.L. Wang, X.R. Feng, Z.Q. Dong, L. Zhang, L.I.U. Yong, Trans. of Nonferrous Metals Society of China **18**, 512-517 (2008) https://doi.org/10.1016/S1003-6326(08)60090-4
12. P. Gao, Z. Wang, Jallcom **854**, 157172 (2021) https://doi.org/10.1016/j.jallcom.2020.157172
13. V.M. Imayev, A.A. Ganeev, D.M. Trofimov, N.J. Parkhimovich, R.M. Imayev, J. MSEA **817** 141388 (2021) https://doi.org/10.1016/j.msea.2021.141388
14. M.N. Mathabathe, R. Modiba, A.S. Bolokang, Surfin **25**, 101173 (2021) https://doi.org/10.1016/j.surfin.2021.101173
15. A.A. Siahboumi, A. Kermanpur, F. Sadeghi, H.R. Ghorbani, 2021. Jallcom **860**, 158437 (2021) https://doi.org/10.1016/j.jallcom.2020.158437
16. Q. Xu, H.Z. Fang, C. Wu, Q. Wang, H.Z. Cui, R.R. Chen, China Foundry **17**, 416-422 (2020) https://doi.org/10.1007/s41230-020-0099-y
17. L.H. Ye, H. Wang, G. Zhou, Q.M. Hu, R. Yang, Jallcom **819**, 153291 (2020) https://doi.org/10.1016/j.jallcom.2019.153291
18. N. Cui, Q. Wu, Z. Yan, H. Zhou, X. Wang, Mat. **12**, 2757 (2019) https://doi.org/10.3390/ma12172757
19. M. Kastenhuber, B. Rashkova, H. Clemens, S. Mayer, Intermet **63**, 19-26 (2015) https://doi.org/10.1016/j.intermet.2015.03.017
20. S. Karthikeyan, M.J. Mills, Intermet **13**, 985-992 (2005) https://doi.org/10.1016/j.intermet.2004.12.020
21. A. Knaislová, P. Novák, F. Průša, M. Cabibbo, L. Jaworska, D. Vojtěch, Jallcom **810**, 151895 (2019) https://doi.org/10.1016/j.jallcom.2019.151895
22. J.H. Lee, H.K. Park, J.H. Kim, J.H., Jang, S.K. Hong, I.H. Oh, JMRT **9**, 2247-2258 (2020) https://doi.org/10.1016/j.jmrt.2019.12.056
23. M. Tlotleng, JMEP **28**, 701-708 (2019) https://doi.org/10.1007/s11665-018-3789-5
24. F. Appel, M. Oehring, J.D.H. Paul, J. Msea **493**, 232-236. (2008) https://doi.org/10.1016/j.msea.2007.08.095
25. Y. Liu, W. Liu, Y. Ma, C. Liang, C. Liu, C. Zhang, Q. Cai, J. Surfcoat **353**, 32-40 (2018) https://doi.org/10.1016/j.surfcoat.2018.08.067
26. X. Lan, H. Wu, Y. Liu, W. Zhang, R. Li, S. Chen, X. Zai, T. Hu, J. Matchar **120**, 82-89 (2016) https://doi.org/10.1016/j.matchar.2016.08.026